Morphological ordering the organic layer for high-performance hybrid thermoelectrics

Lin Yang,[1,2*] Yi Tao,[3] Madeleine P. Gordon,[4,5] Akanksha K. Menon,[2,6] Ravi S. Prasher,[2,7*] Jeffrey J. Urban[5*]

[1]Department of Advanced Manufacturing and Robotics, Peking University, Beijing 100871, China.

[2]Energy Storage and Distributed Resources Division, Lawrence Berkeley National Laboratory, Berkeley, CA, 94720, USA.

[3]School of Mechanical Engineering and Jiangsu Key Laboratory for Design and Manufacture of Micro-Nano Biomedical Instruments, Southeast University, Nanjing, 210096, P. R. China.

[4]Applied Science and Technology Graduate Group, University of California, Berkeley, CA, 94720, USA.

[5]The Molecular Foundry, Lawrence Berkeley National Laboratory, Berkeley, CA, 94720, USA.

[6]George W. Woodruff School of Mechanical Engineering, Georgia Institute of Technology, Atlanta, GA 30332, USA

[7]Department of Mechanical Engineering, University of California, Berkeley, CA, 94720, USA.

*Corresponding author. Email: linyangpku@pku.edu.cn; RSPrasher@lbl.gov; jjurban@lbl.gov

Abstract: Inorganic-organic hybrids, such as Te-PEDOT:PSS core/shell nanowires, have emerged as a class of promising thermoelectric materials with combined attributes of mechanical flexibility and low cost. However, the poorly understood structure-property relationship calls for further investigation for performance enhancement. Here, through subsequent focused electron beam irradiation and thermal annealing treatments on individual Te-PEDOT:PSS nanowires, the measured thermoelectric properties provide an unprecedented evidence confirming the dominant role of organic shell on charge transport. These are strongly supported by Kang-Snyder model and molecular dynamics simulations, which offer mechanistic insights in terms of heating enabled morphological ordering of the polymer chains. Our results show that thermal annealing at 450 K on the 42 nm nanowire results in a *ZT* value of 0.78 at 450 K. Through leveraging the interfacial self-assembly of organic phase to construct a high electrical conductivity domain, this work lays out a clear framework for development of next-generation soft thermoelectrics.

Introduction

Organic-inorganic hybrid materials have recently been shown to exhibit high electrical conductivity σ, high Seebeck coefficient S, and low thermal conductivity κ, simultaneously that leads to a promising thermoelectric performance ($ZT = S^2 \sigma T / \kappa$).[1–4] In contrast to simple composites with behavior that is often an average of that of the constituent materials, hybrid materials capitalize on interfacial properties to yield gains in performance exceeding that of the individual components.[3,5] Over the past decade, the accelerated pace of development of hybrid materials has led to a surge of interest in applications beyond what is currently possible with traditional inorganic counterparts - such as flexible heating-cooling devices,[6] wearable electronics,[7,8] and foldable organic light-emitting diodes (OLEDs).[9,10] However, one challenge associated with this emerging class of thermoelectric material is the lack of a fundamental understanding of the unique structure-property relationships and the underlying complex carrier physics, which are critical to promoting the commercial deployment of hybrid electronics.

Among different hybrid thermoelectric materials, tellurium-poly(3,4-ethylenedioxythiophene):poly(styrenesulfonic acid) (Te-PEDOT:PSS) core/shell nanowires are the most well-studied system owing to their favorable thermoelectric performance,[1,11–14] where a *ZT* value of ~ 0.39 at 300 K was achieved after chemical treatment with sulfuric acid[15], and a higher *ZT* of 0.54 was reached for a single nanowire at 400 K.[16] There are a number of hypotheses regarding the physics underlying this remarkable thermoelectric performance,[12–15,17–19] but the structural and energetic complexities of this hybrid material make definitive conclusions challenging. Recent theoretical calculations inferred that the thin organic shell dominates electrical transport due to the physical templating effect that induces ordering of PEDOT

domains on the inorganic core.[5,20] This was later experimentally shown through thermoelectric property measurements on individual hybrid nanowires with different Te core diameters and a fixed organic shell thickness - an inverse relationship between κ and σ with respect to nanowire diameter supports predictions that electrical transport occurs through the organic shell while thermal transport is driven by the inorganic core.[16] However, this serves as an indirect experimental evidence for the dominate role of PEDOT:PSS in charge transport, thus requiring a more direct and conclusive investigation that unravels the charge carrier transport mechanism. Confirmation of charge transport occurring primarily though the organic shell would then focus research efforts on engineering the polymer shell to enhance thermoelectric transport in hybrid materials.

From the classical Drude model framework, the electrical conductivity of an organic material can be improved with a high carrier mobility (through better ordering of the molecular chains), or by increasing the charge carrier concentration (via doping).[2,4,21–23] However, the effects of doping on the electronic properties of organic materials are multifaceted[2] - for example, dopants can cause distortions in the intermolecular packing of the semiconductor that reduces the charge carrier mobility,[24–26] and the incorporation of large amounts of dopant can even lead to phase segregation of the doped phase from the undoped phase[27,28] – all of which severely lowers σ. Doping is even less favorable for a hybrid material in which the physical templating effect creates morphological order in the thin organic shell on the inorganic core.[5,16] In this case, any structural distortion resulting from doping may result in a loss of this unique interaction that occurs at the hard-soft interface.

On the other hand, carrier mobility can be tuned via structure and morphology modifications through a myriad of ways,[29–37] for example thermal annealing and electron beam (e-beam) irradiation. Low temperature (< 200 ℃) thermal annealing can improve the charge carrier mobility by modifying the molecular structure and orientation, as well as facilitating coalescence between the granular conductors, collectively leading to a higher σ.[29–34] In contrast, low voltage e-beam irradiation has been shown to disrupt the molecular chain alignment of polymer thin films, leading to cluster formation and charge localization.[35–37] Furthermore, swelling of the granular conductors increases the inter-grain distance and hopping barriers,[37] which drastically reduces the carrier mobility and σ. As discussed later, for the case of Te/PEDOT:PSS hybrids, the Te core is essentially insensitive to thermal annealing at these low temperatures and e-beam irradiation. Thus, thermoelectric property measurements on the same hybrid nanowire undergoing subsequent annealing (improves σ) and irradiation (reduces σ) treatments could provide a more direct evidence on the role of the organic shell and inorganic core in charge and heat transport, respectively. Moreover, thermal annealing can be performed as a post-processing step that further enhances the structural order and crystallinity of the polymer shell that is aligned along the Te core during synthesis.

In this work, we investigate the effects of annealing on individual Te-PEDOT:PSS core/shell nanowires using *in-situ* thermoelectric properties measurements. Focused electron beam irradiation on a Te-PEDOT:PSS hybrid nanowire and subsequent thermal annealing of the same nanowire demonstrates that electrical transport is predominantly driven by the organic shell, and that thermal annealing is able to enhance electrical transport through a reordering of the polymer chains. This direct experimental evidence is strongly supported by molecular dynamics (MD)

simulations, and it offers mechanistic insights on the heating enabled morphological ordering of polymer chains. Our results show that thermal annealing at 450 K on a 42 nm nanowire increases *ZT* by a factor of 1.3× at 300 K, and results in a *ZT* value of 0.78 at 450 K, which represents the highest *ZT* ever reported at this temperature for hybrid materials.

Results

Thermoelectric measurement scheme and thermal annealing treatment. The nanowires used in this study consist of a soft polymer shell (PEDOT:PSS) and a hard inorganic core (Te) (details on nanowire synthesis in Methods), where the shell thickness is ~1.5 nm, while the core diameter is varied.[16] The electrical conductivity, Seebeck coefficient and thermal conductivity of the same individual Te-PEDOT:PSS core/shell nanowire was measured using a custom-fabricated suspended microdevice platform.[38–40] Fig. 1a shows a single Te-PEDOT:PSS nanowire between two suspended membranes with integrated platinum (Pt) coils serving as resistance heaters and thermometers and additional Pt electrodes. To eliminate the effects of contact resistance in thermal/electrical conductivity measurements, electron beam induced deposition (EBID) is used to locally deposit Pt/C composite at the contacts between the nanowire and underlying Pt electrodes, as shown in Fig. 1a.[41] More details on the device fabrication and measurement techniques can be found in Methods.[42–44]

To explore the effects of thermal annealing on the transport properties of Te-PEDOT:PSS nanowires, a 186 nm diameter sample was measured under a temperature ramp from 300 to 400 K. After placing the nanowire sample at 400 K for 2 hours, the temperature was ramped down and the measurements were conducted again with a 10 K interval until 300 K. A slow

heating/cooling rate of 2 K/min was used to ensure that all measurements are performed in a state of thermal equilibrium. This long heating duration and slow cooling process also provides sufficient time for the morphological changes in the polymer chains to occur, thereby leading to an improvement in the crystallinity.[30] Note that all the measurements were conducted in a cryostat under high vacuum conditions (<10^{-6} mbar), and thus the effects of moisture as well as oxygen are not important in the annealing process. Before the annealing process was performed, the nanowire sample was stabilized in this vacuum environment for 2 hours.

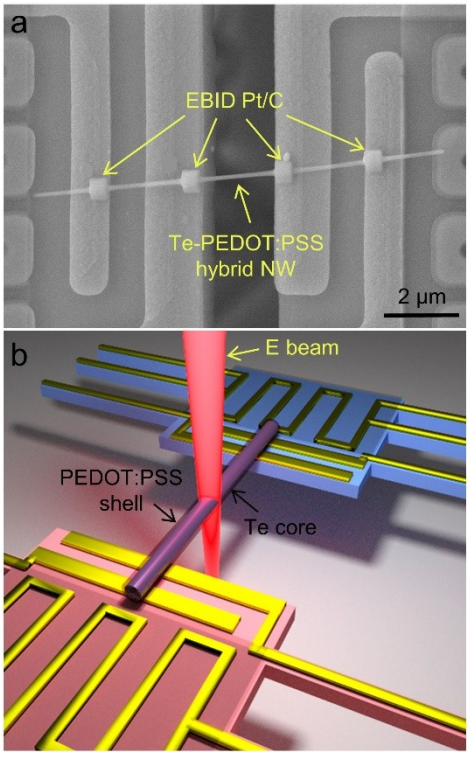

Figure 1. **Thermoelectric measurement with suspended microdevice and electron beam irradiation treatment.** (a). SEM image showing the suspended microdevice with a Te-PEDOT:PSS hybrid nanowire placed between two membranes for thermoelectric properties measurements. Pt/C was locally deposited via electron-beam-induced deposition (EBID) at the contacts between the nanowire and the four electrodes to enhance the thermal/electrical contact. The electrical resistance of the individual nanowires is measured using the four-probe method, and the Seebeck coefficient is measured simultaneously with thermal conductivity measurements. (b) Schematic showing the hybrid nanowire placed on the measurement device undergoing focused electron beam irradiation treatment.

Measured thermoelectric properties after subsequent electron beam irradiation and thermal annealing treatments. The measured results are shown in Fig. 2b-d. As expected, the measured σ values for the same sample before and after annealing at 400 K are different. Electrical conductivity of the 186 nm Te-PEDOT:PSS nanowire at 300 K increases from 11.7 S/cm to 16.5 S/cm after being annealed at 400 K, representing a 1.4× enhancement. In contrast, the measured S at the same temperature is 280 and 292 μV/K before and after the annealing process, which is within the inherent measurement uncertainty. This reveals that thermal annealing improves σ and poses a negligible effect on S; this is a desirable outcome as S and σ are often coupled.

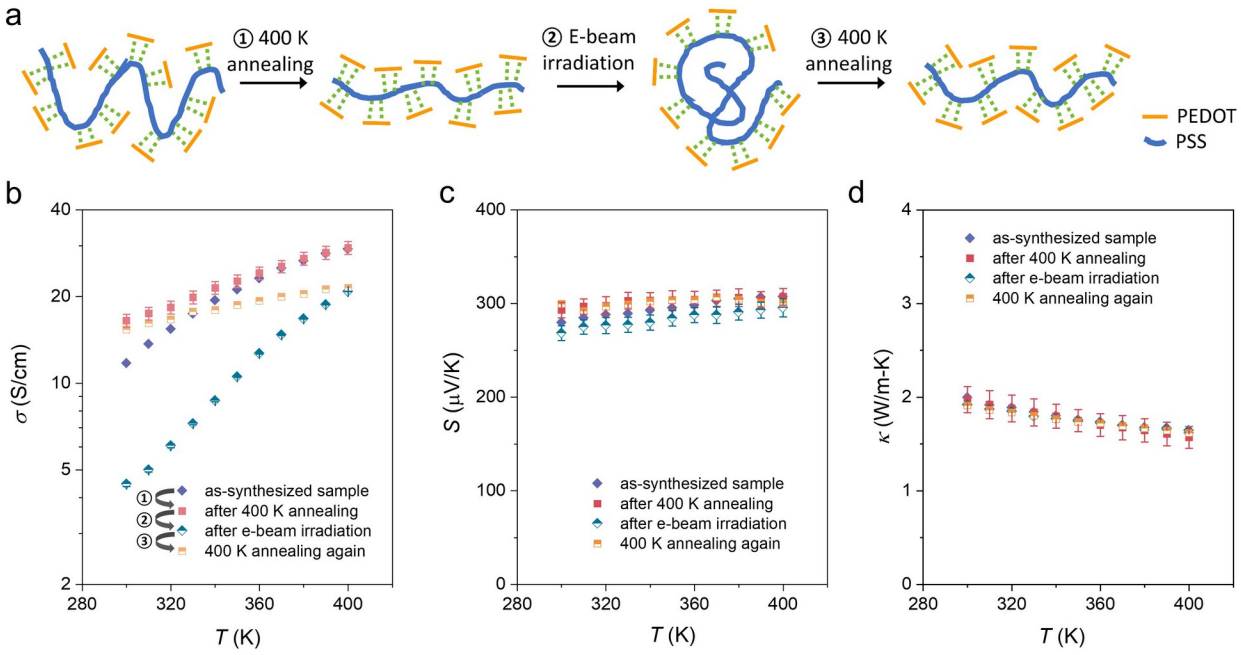

Figure 2. Measured thermoelectric properties after subsequent annealing and e-beam irradiation treatments. (a) Schematic showing the molecular morphology and chain alignment change in the PEDOT:PSS shell after thermal annealing and e-beam irradiation. Temperature-dependent (b) electrical conductivity, (c) Seebeck coefficient, and (d) thermal conductivity for the same 186 nm diameter Te-PEDOT:PSS nanowire sample after each treatment. Here, the measurement uncertainties of σ and κ are mainly from the uncertainties in nanowire length and diameter measurements, and uncertainties in S are mainly from the uncertainties in linear least squares fitting.

Given that the melting point of Te is ~718 K,[45] the relatively low temperature annealing treatment should not affect the electrical properties of the inorganic Te core. In contrast, gazing incidence X-ray diffraction has shown that annealing at ~400 K can largely improve the molecular chain alignment of PEDOT:PSS thin films, leading to enhanced crystalline order.[29,30] Moreover, the heating effect was recently quantified by measuring the backbone alignment through the orientational correlation length (OCL) using polarized resonant soft x-ray scattering (RSoXS), with the OCL increasing after thermal processing and reaching ~180 nm for PBTTT films annealed at 180 ℃.[46] We thus hypothesize that thermal annealing improves σ through better ordering the polymer chains (improves charge carrier mobility) in this organic-inorganic hybrid material.

To validate our hypothesis and provide a more direct evidence on the dominant role of the organic shell on charge transport, low energy e-beam irradiation was conducted on the same 186 nm diameter sample (see Methods for more details), and thermoelectric properties are measured again (Fig. 2b-d). It has been previously shown that e-beam irradiation could disrupt the polymer chains and cause charge localization.[35–37] Indeed, although thermal annealing increases σ to 16.5 S/cm for this 186 nm sample, the values is drastically reduced to 4.5 S/cm at 300 K after e-beam treatment. Interestingly, annealing this irradiated nanowire again at 400 K successfully restores the structural order of the thin polymer shell, bringing the σ back to 15.4 S/cm (a similar trend is also observed in an 85 nm hybrid nanowire, Supplementary Information Note 3). It is worth noting that all measurements are performed on the same nanowire sample, which rules out any complexity due to any sample variations. Meanwhile, the low voltage e-beam irradiation is unlikely to pose any effect on the inorganic Te core. Thus, this well-controlled electrical

transport property measurement provides previously unavailable evidence that confirms the dominant role of PEDOT:PSS shell on charge carrier transport by means of structural ordering of polymer chains during annealing, and similar to the annealing effects, e-beam irradiation also poses negligible effects on the Seebeck coefficient (Fig. 2c).

Next, thermal conductivity measurements on these same hybrid single nanowire samples reveal that they all possess essentially the same κ despite significant differences in the shell morphology, as Fig. 2d demonstrates. Note that an effective way of increasing polymer thermal conductivity is through improving the crystallinity by means of electrospinning[36] or ultra-drawing;[47] thus if the polymer shell contributes to thermal transport, we would expect to see variations in κ after the nanowire is subjected to e-beam irradiation and thermal annealing. Since this is not the case and the nanowire shows overlapping κ values for these four measurements, it indicates that the Te core is predominantly responsible for thermal transport. Moreover, given with the variation in the measured σ, the nearly constant κ suggests that phonons are the main thermal energy carriers with little contribution from electrons in this hybrid material. This finding is consistent with our recent work that showed the separation of electron and phonon transport channels in Te-PEDOT:PSS core/shell nanowires.[16] Note that the nearly constant κ before and after annealing as well as e-beam irradiation suggests that there is minimal structural change to the Te core, and we are thus able to successfully modulate the structure of the PEDOT:PSS shell with core being intact.

Kang-Snyder model and MD simulation to reveal the annealing effects. To better understand charge carrier transport in the hybrid nanowire undergoing these different treatments, Kang-Snyder model is used to fit the measured temperature-dependent σ and S of the same 186 nm

diameter nanowire. The Kang-Snyder model is a generalized model to describe charge transport in various conducting polymers over a wide temperature range.[48] The key equations from the Kang-Snyder model are

$$\sigma = \sigma_{E0}(T) \times sF_{s-1}(\eta), \tag{1}$$

$$S = \frac{k_B}{e}\left[\frac{(s+1)F_s(\eta)}{sF_{s-1}(\eta)} - \eta\right], \tag{2}$$

with the non-normalized complete Fermi-Dirac integral $F_i(\eta) = \int_0^\infty \frac{\varepsilon^i}{1+e^{\varepsilon-\eta}} d\varepsilon$. Here, the transport coefficient $\sigma_{E0}(T)$ is a temperature-dependent but energy-independent parameter, which is related to charge carrier mobility. s is the empirical parameter characterizing the polymeric system that equals 1 for PEDOT.[5,48] The reduced chemical potential is $\eta = (E_F - E_t)/k_BT$, where E_F is Fermi level, E_t is transport energy, below which there is no contribution to the conductivity, k_B is Boltzmann constant, and T is the absolute temperature.

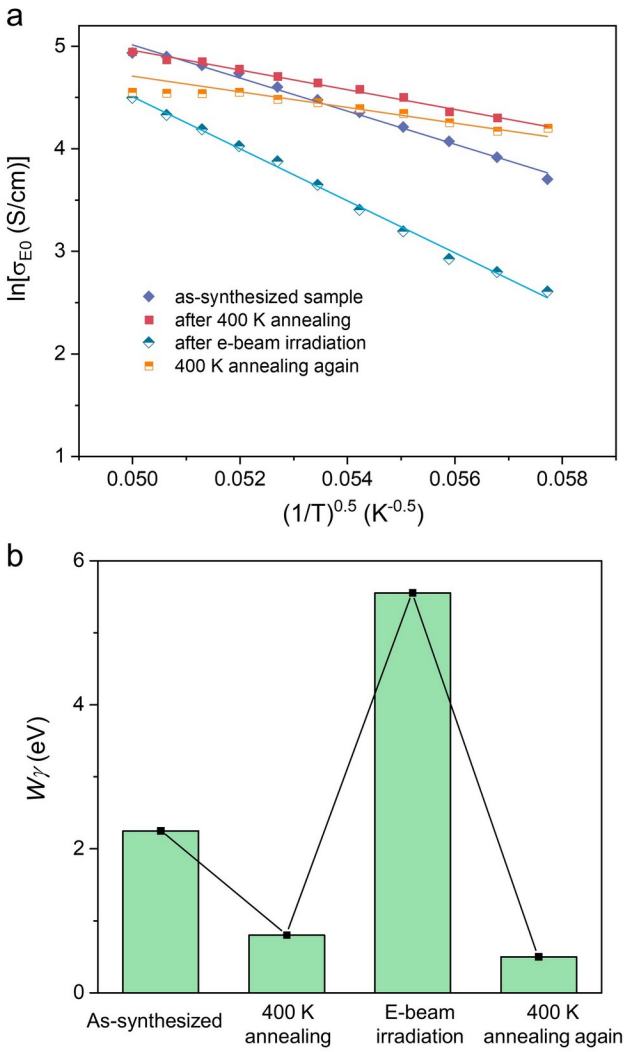

Figure 3. **Kang-Snyder model on electrical transport properties.** (A and B) Measured temperature-dependent Seebeck coefficient and electrical conductivity of Te-PEDOT:PSS hybrid nanowires with different diameters. (C) Reduced chemical (a) Based on the Kang-Snyder model, the transport coefficient σ_{E0}, which relates with the charge carrier mobility, is extracted based on the measured electrical properties, and $\ln(\sigma_{E0})$ is plotted as a function of $T^{-0.5}$ for the 186 nm Te-PEDOT:PSS nanowire after each treatment. (b) Hopping energy W_γ is extracted by taking the slope of $\ln(\sigma_{E0})$ versus $T^{-0.5}$ curve for the four different sample conditions, which represents the energy barrier for the intercrystallite carrier transport within the polymer shell.

It is well known that the Seebeck coefficient of a material is strongly dependent on its carrier density, and the nearly constant S in Fig. 2c indicates that carrier concentration does not vary with the different treatments for the same Te-PEDOT:PSS nanowire. This also suggest that the

enhanced carrier mobility is the driver for the enhanced electrical conductivity. Fig. 3a shows the calculated $\sigma_{E0}(T)$ based on the measured Seebeck coefficient and electrical conductivity for the 186 nm nanowire using Eqs. (1-2). σ_{E0}(300 K) increases from 40.4 to 66.6 S/cm after the first annealing treatment at 400 K. However, σ_{E0}(300 K) drastically reduces to 13.5 S/cm due to the molecular chain disruption caused by the focused e-beam irradiation, and then increases back to 62.6 S/cm after another round of thermal annealing. A high value of the transport coefficient σ_{E0} indicates an enhanced carrier mobility, and the variation in the calculated σ_{E0} is a result of the modulated structural ordering of polymer chains under the different treatment conditions.

Based on the physical picture of inhomogeneous disorder model, $\sigma_{E0}(T)$ is proportional to $\exp\left[-\left(\frac{W_\gamma}{k_B T}\right)^{1/2}\right]$, where W_γ is the energy barrier for intercrystallite carrier transport, and it should decrease with improved morphology.[48,49] Indeed, Fig. 3b plots the extracted W_γ value for the same nanowire under four different treatment conditions, which first reduces from 2.25 to 0.79 eV due to thermal annealing, then increases to 5.55 eV due to the e-beam irradiation induced structural disruption, and finally reduces to 0.5 eV after the second round of thermal annealing. This can be understood as, apart from reorienting the polymer chains, heating may also affect the colloidal particle interaction in PEDOT:PSS.[29] It is known that σ of PEDOT:PSS films depends critically on the size distribution and connectivity of the constituent granular conductors. Elevated temperature annealing leads to coalescence of PEDOT:PSS grains as well as improved ordering of the granular conductors, which reduces the number as well as the height of the inter-grain hopping barriers.[29] Taken together, our results suggests that annealing at elevated temperature

improves the morphological order as well as the crystallinity of the organic shell, which in turn leads to the enhanced σ of the hybrid nanowire.

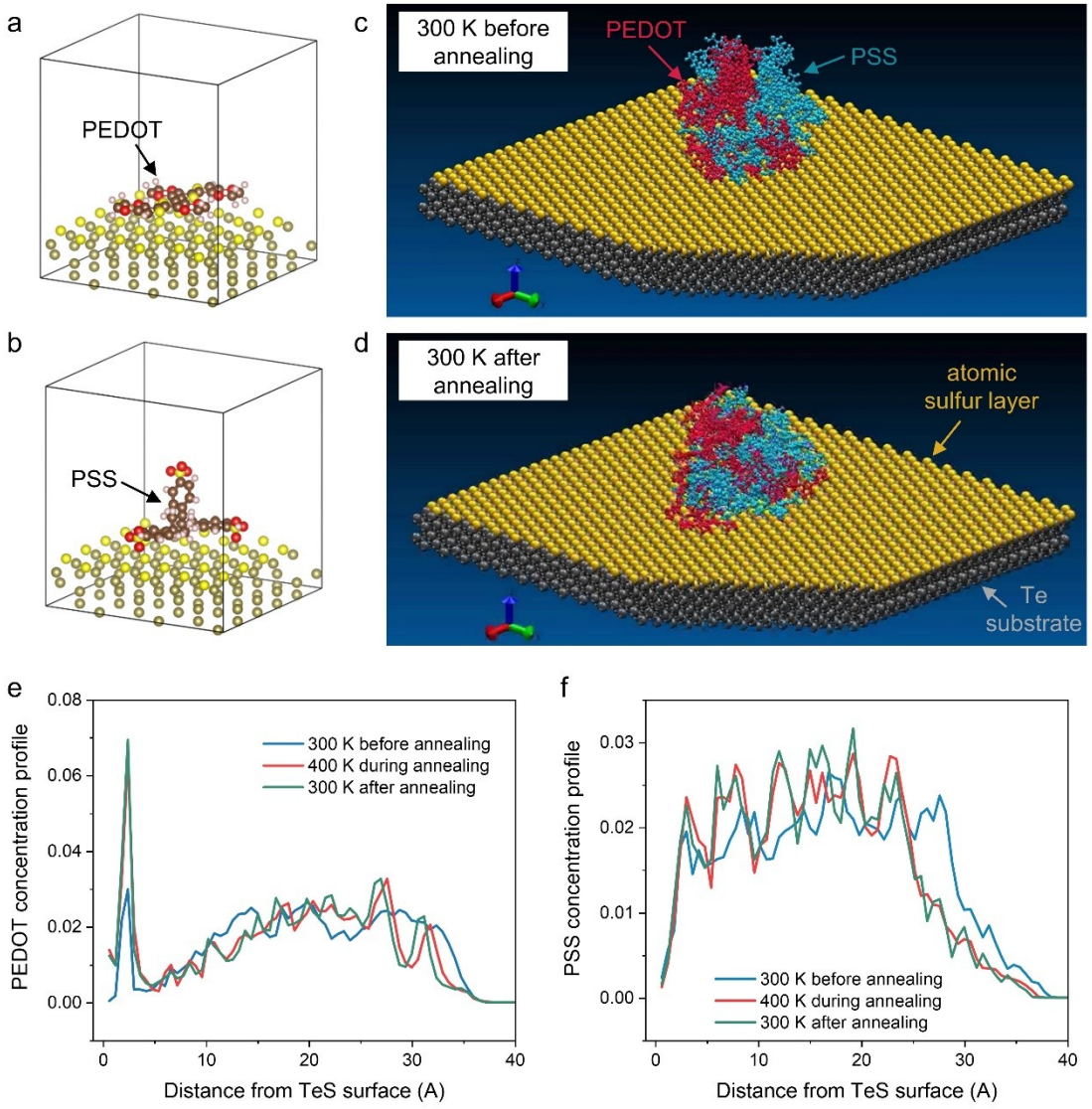

Figure 4. MD simulation reveal annealing effects on the alignment of PEDOT at the inorganic interface. Schematic of (a) PEDOT/TeS, and (b) PSS/TeS for interface adsorption energy calculations using density functional theory (DFT). Note that TeS represents an atomic layer of sulfur on the surface of Te nanowire due to the synthesis procedures of Te-PEDOT:PSS nanowires (more details in Methods). Molecular dynamics simulation of PEDOT:PSS on TeS surface for (c) initial condition and (d) after 400 K annealing, which elucidates the polymer morphology and alignment at the organic-inorganic interface. Respective atomic concentration profile of (e) PEDOT and (f) PSS is plotted as a function of distance from TeS surface. There is a high concentration of PEDOT chains observed at 2–4 Å from the TeS surfaces, and the peak magnitude further increases after 400 K heating treatment, suggesting thermal annealing

improves the order and alignment of PEDOT chains at the organic-inorganic interface. In contrast, PSS molecules exhibit a nearly uniform random distribution both before and after the annealing treatment (Supplementary Movie 1).

To provide mechanistic insights into the annealing effects, molecular dynamics (MD) simulations are performed to study the morphological ordering of PEDOT chains on the inorganic nanowire surface under heating. Note that there is an ultra-thin layer of sulfur (*S*) on the Te nanowire surface (more details on the TeS surface can be found in Methods). Using density functional theory (DFT), we first calculate the adsorption energy between PEDOT/PSS on the surface of Te with an atomic layer of *S* on top (Fig. 5a-b, details in Methods). Then, MD simulations are conducted to reveal self-alignment of PEDOT chains (Fig. 5c-d, Methods).

It can be seen from the concentration profiles (Fig. 5 e-f) that, even without thermal annealing, there is self-alignment of PEDOT chains 2–4 Å from the TeS surfaces while the PSS remains unaligned, which is consistent with observations in a recent MD simulation.[5] This could be explained by the stronger adsorption energy between PEDOT and TeS (2.37 eV) than that of PSS and TeS (1.05 eV), which indicates a thermodynamic driving force for self-assembly of PEDOT over PSS on the nanowire surface. More interestingly, upon heating the structures to 400 K, more PEDOT moieties tend to align in a planar configuration on the inorganic surface while PSS remains unchanged, as evidenced by the concentration profiles (Fig. 5c-d). The more ordered PEDOT chains after the heat treatment maintain their configuration even after cooling down to 300 K (Fig. 5c-d, Supplementary Movie 1). Thus, these simulations reveal that heating promotes the ordering of PEDOT chains on the inorganic surface and enhances structure crystallinity, which explains the measured higher electrical conductivity after thermal annealing and is in line with the Kang-Snyder model results.

Thermal annealing on a thin hybrid nanowire. After confirming that thermal annealing is a viable approach to improve the electrical transport properties of Te-PEDOT:PSS nanowires, we extend this approach to a thinner nanowire (42 nm) and study the resulting thermoelectric performances. In our recent work we have shown that for smaller diameter wires, the lower interfacial interaction energy at the inorganic/organic interface promotes the physical templating effect of the PEDOT chains, resulting in a larger charge carrier mobility. As such, if thermally annealing the thin nanowire is able to further increase the electrical conductivity, we are able to optimize the *ZT* value of these hybrid nanowires without any complicated chemical doping procedures. As shown as in Fig. 4a, σ(300 K) increases from 42.9 to 48.4 S/cm after the first round of thermal annealing, representing a 1.13× enhancement. This is smaller than that of the 186 nm sample (~1.4×), which is likely due to an already improved alignment of PEDOT chains on thinner Te core nanowires. Similar to the 186 nm diameter sample, Fig. 4b shows that the measured *S* remains roughly constant for the two measurements (309 and 313 μV/K).

Previous annealing studies on undoped PEDOT:PSS thin films show that σ(300 K) increases monotonically as annealing temperature increases up to 473 K, after which σ(300 K) starts to decrease due to irreversible structural degradation of the polymer chains.[30] To examine whether we are able to further increase the electrical conductivity, the thermoelectric properties of the same 42 nm diameter sample were measured again from 450-300 K after annealing at 450 K for 2 hours. As shown in Fig. 4a, the measured σ is consistently higher than the measured value after 400 K treatment with σ(300 K) reaching 51.8 S/cm, while *S* and κ still remain largely unchanged. Taken together, when compared with the original thermoelectric power factor ($PF = S^2\sigma$) of 410.7 μW/m-K^2 at 300 K without annealing, the *PF* of the same 42 nm nanowire reaches 541.9

μW/m-K^2 after the 450 K thermal annealing. This translates to a *ZT* enhancement from 0.18 to 0.24 at 300 K, and a *ZT* of 0.78 is achieved at 450 K, which represents the highest *ZT* value achieved for hybrid materials.

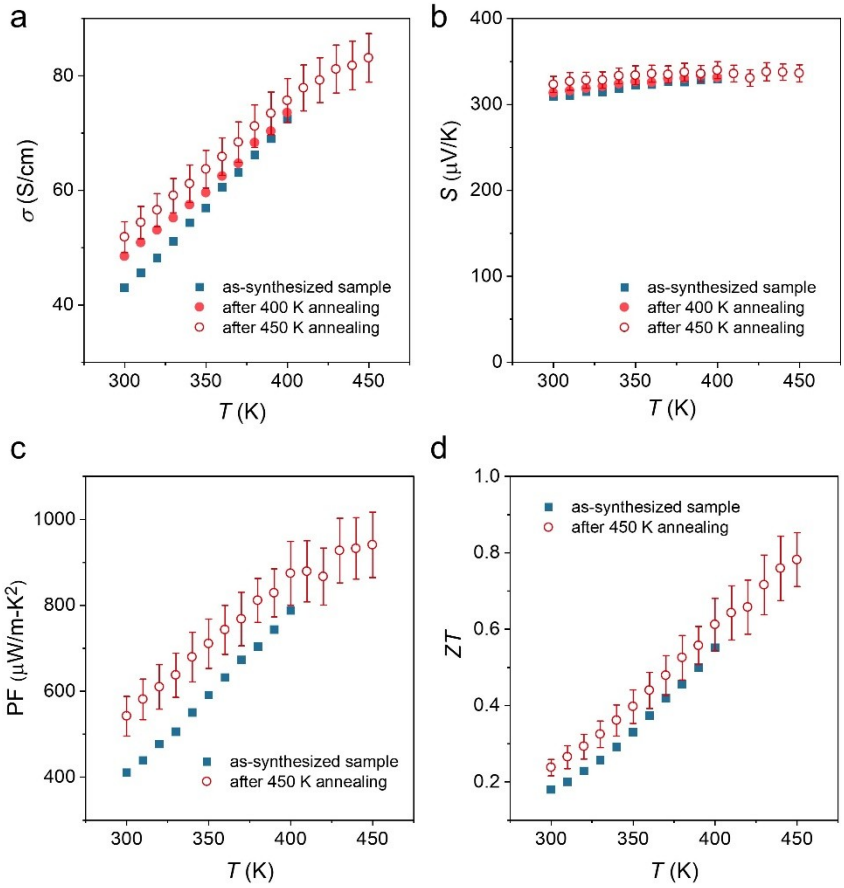

Figure 5. Annealing effects on a thin hybrid nanowire. Measured temperature-dependent (a) electrical conductivity, (b) Seebeck coefficient of a 42 nm diameter Te-PEDOT:PSS nanowire as-synthesized and after 400 K as well as 450 K thermal annealing treatments. Measured temperature-dependent (c) thermoelectric power factor ($PF = S^2\sigma$), and (d) thermoelectric figure of merit *ZT* for the as-synthesized wire, and after a 450 K annealing treatment. Here, the measurement uncertainties of σ are mainly from the uncertainties in nanowire length and diameter measurements, uncertainties of *S* are mainly from the uncertainties in linear least squares fitting, and the uncertainties of *PF* and *ZT* are calculated on the basis of the respective uncertainties in *S*, σ, and κ.

To rule out any uncertainties related with measurement techniques, we measured thermoelectric properties of Te-PVP nanowires undergoing the exact same annealing procedures, where the measured σ, S, and κ all exhibit nearly identical values before and after annealing at

450 K (see Supporting Information Note 4). Notably, different from PEDOT:PSS, PVP is an electrical insulator, and electrical transport only occurs in Te core. Therefore, the unchanged thermoelectric properties with this insulating shell clearly indicate that thermal annealing does not affect the transport properties of Te, and our measurement setup exhibits good thermal stability. This in turn confirms that thermal annealing is able to improve the structural order of PEDOT, and also justifies that PEDOT:PSS is the primary electrical transport channel in Te-PEDOT:PSS hybrid nanowires. It is important to point out that the measured σ of the Te-PVP nanowire is very close to the measured σ of the 186 nm Te-PEDOT:PSS nanowire after e-beam irradiation (Fig. S3a), which indicates that for Te-PEDOT:PSS nanowire with disrupted molecular configurations in the organic shell, the inorganic Te core becomes the primary charge conductor.

Discussion

By comparing the measured thermal/electrical conductivity and Seebeck coefficients with subsequent treatment using thermal annealing and e-beam irradiation, this work provides unprecedented evidence to confirm the dominant role of the organic shell on charge transport in Te-PEDOT:PSS core/shell nanowires. Through pairing our experimental data with Kang-Snyder model and MD simulations, the improved electrical conductivity after thermal annealing is attributed to better ordered PEDOT chains on the inorganic surface, which enhances polymer crystallinity and structural ordering. This in turn points to a promising strategy to improve the thermoelectric performance of Te-PEDOT:PSS hybrid nanowires, where a *ZT* value of 0.78 is achieved for a 42 nm diameter wire after annealing at 450 K.

Historically, for room-temperature or near-ambient applications, the industry standard thermoelectric material has long been Bi_2Te_3.[50] In the past decade, driven by rapid progress in the field of organic semiconductors, organic-inorganic hybrid nanowires have made large strides in catching up with their inorganic counterparts in terms of thermoelectric performance, particularly for these low-temperature applications.[16,51,52] As such, this work lays out a clear framework for the development of next-generation soft thermoelectrics, that is to create architectures and templates leveraging the interfacial self-assembly of organic phase to enhance the mobility of charge carriers and construct a high electrical conductivity domain. This could serve as the design guidelines for the hybrid materials to further improve their thermoelectric performance and compete with the inorganic counterparts.

Methods

Nanowire synthesis. Synthesis of Te-PEDOT:PSS core/shell nanowires was performed according to the ligand exchange procedure published by Sahu et al. (54). PEDOT:PSS (Clevios PH1000) was purchased from Heraeus and was vortexed and filtered but otherwise underwent no further processing. Tellurium dioxide (99.9995%), PVP (average molecular weight, 40 kDa), sodium hydroxide (Sigma-Aldrich reagent, ≥ 97.0%, pellets), ethylene glycol (ReagentPlus, ≥ 99%), hydrazine hydrate (78 to 82%, iodometric), and sodium sulfide were purchased from Sigma- Aldrich. The single-crystal Te nanowires are initially synthesized with PVP as the surface ligand to act as the structure directing agent. In order to convert the Te-PVP NWs to the more useful form of Te-PEDOT:PSS NWs, a multistep ligand exchange process was employed.[53] The cleaned Te-PVP NWs were placed in a closed jar with excess water and NaS (≈ 1 g). The mixture was left to stir overnight. The next morning the NW solution was cleaned thrice following the centrifugation protocol detailed in Ref.[53]. After this step, the cleaned NWs were coated with an ultra-thin layer of sulfide, and were then suspended in excess water with PEDOT:PSS (≈ 10 mL) added to the solution. The mixture was again stirred and left overnight. After stirring overnight, the PEDOT:PSS-NW solution was cleaned again thrice via centrifugation to yield clean Te-PEDOT:PSS NWs. Hybrid nanowires are then drop-casted onto glass substrates.

Thermoelectric property measurements on individual nanowires. For thermoelectric measurements, the hybrid nanowire meshes were first immersed in reagent alcohol and sonicated for ~10 s, and the nanowire suspension was then drop-casted on a piece of polydimethylsiloxane (PDMS). Next, an individual nanowire was picked up by a sharp probe, mounted on an in-house

assembled micromanipulator, and laid between two side-by-side suspended membranes integrated with microheaters/thermometers. The thermoelectric properties of individual nanowires were measured in a cryostat (Janis VPF-800) operated under a high vacuum ($<1\times10^{-6}$ mbar) with a dual radiation shield configuration. EBID (electron beam induced deposition) of the Pt/C composite was performed at the contacts between the nanowire and Pt electrodes using a dual-beam system (focused ion beam–scanning electron microscope, FEI Quanta) to establish good electrical contacts and minimize the contact thermal/electrical resistance.

The electrical resistance measurement was performed before thermal measurements at each designated temperature point using the four-probe method. During the measurements, we used a DC voltage output from the data acquisition board (National Instruments PCI-6052e), which was connected to a large resistor (1 megohm) in series with the outer electrodes of the microdevice. By varying the output DC voltage, a sweeping DC current was applied to the Te-PEDOT:PSS nanowire, with the voltage difference between the two inner electrodes measured by a voltage amplifier (Stanford Research Systems, SR560), and the DC current was recorded by a high-accuracy current amplifier (Keithley 6487). The temperature-dependent electrical resistance [R(T)] of each measured sample is subsequently obtained by fitting the linear I-V curve.

To increase the sensitivity for thermal connectivity measurements, a Wheatstone bridge circuit was adopted through introducing a blank device, which helps to reduce the noise from the tempera- ture fluctuations of the sample holder. During the thermal measurements, we also measured the Seebeck coefficient for each sample by monitoring the temperature difference of the two suspended membranes and the induced voltage difference (SR560) across the two inner electrodes.

Electron beam irradiation on nanowires. To disrupt the molecular structure of PEDOT:PSS shell, we use e-beam to irradiate the suspended portion of the Te-PEDOT:PSS hybrid nanowire across two measurement islands. The suspended length is imaged and irradiated through FEI Quanta Scanning Electron Microscope under an accelerating voltage of 5 kV for 6 s.

Density function theory for adsorption energy calculation. The density functional theory (DFT) calculations are used to calculate adsorption energies of PEDOT/PSS on the surface of TeS. The Vienna ab initio simulation package (VASP) is prepared for DFT calculations. The Energy cutoff of 520 eV is chosen for the plane wave basis sets in the projector augmented wave (PAW) method. The exchange correlation interaction is treated with local density method. For TeS film, the 22.56 Å x 23.45 Å x 5.96 Å Te [100] film is constructed with 28 Å vacuum region, and a single atomic layer of S is absorbed on the top of Te film with the optimized equilibrium separation of 1.09 Å. Then, PEDOT4 and PSS3 are placed on the top of TeS film as shown in Fig. 4a-b, which have similar numbers of atoms and the same carbon atoms number of 24. The equilibrium separations between PEDOT/PSS and TeS are optimized to guarantee the whole system has the lowest energy. After optimization, the adsorption energy is calculated as follows:

$$E_{adsorption} = E_{total} - E_{PEDOT/PSS} - E_{TeS} \quad (1)$$

where E_{total}, $E_{PEDOT/PSS}$ and E_{TeS} represent the energy of the whole system, isolated $PEDOT/PSS$ and TeS, respectively. The optimized equilibrium separations and adsorption energies between $PEDOT/PSS$ and TeS are presented in Supplementary Table 1.

Molecular dynamic simulation for thermal annealing treatment. The molecular dynamics (MD) is used to simulate the adsorption process of PEDOT:PSS on the TeS substrate using LAMMPS package. The bond and angle interactions are modeled by harmonic potential for the PEDOT:PSS, while the dihedral interactions are modeled by Optimized Potentials for Liquid Simulations (OPLS) force field and the improper interactions are modeled by Consistent Valence Force Field (CVFF) for the PEDOT:PSS. The interactions between PEDOT:PSS and TeS are modeled by Lennard-Jones (LJ) potential with the parameters extracted from the previous DFT calculations. At the beginning, twenty PEDOT4 and eight PSS8 are mixed and laid on the surface of TeS. During the simulations, the velocity Verlet algorithm with a time step size of 0.1 fs is used for the integration of the motion equations. The PEDOT:PSS is first equilibrium at 300 K for 0.1 ns. After the system reaches thermal equilibrium, the PEDOT:PSS is heated up to 400 K for 0.1 ns. Then, the PEDOT:PSS is annealed at 400K for 0.5 ns. Later, the PEDOT:PSS is cooled down to 300 K for 0.1 ns. Finally, the PEDOT:PSS is equilibrium again at 300 K for another 0.1 ns.

Supplementary Information

Supplementary Information of this article is available.

Acknowledgements

L. Y. acknowledges the support from Peking University College of Engineering. This work was partially performed at the Molecular Foundry, Lawrence Berkeley National Laboratory, and was supported by the Department of Energy, Office of Science, Office of Basic Energy Sciences, Scientific User Facilities Division of the U.S. Department of Energy under contract no. DE-AC02-05CH11231.

Author contributions

L.Y. conducted focused electron beam irradiation and thermal annealing on individual hybrid nanowires, as well as thermoelectric property measurements. L.Y. performed thermoelectric modeling using the Kang-Snyder model. Y. T. conducted DFT calculation and MD simulation. M.P.G. synthesized Te-PEDOT:PSS and Te-PVP hybrid nanowires. L.Y. compiled and analyzed

results. L.Y., J.J.U., and R.S.P. conceived and directed the project. L.Y. and A.K.M. wrote the manuscript with input from all authors.

Competing Interests

The authors declare that they have no competing interests.

Data and materials availability

All data needed to evaluate the conclusions in the paper are present in the paper and/or the Supplementary Information.

References

1. See, K. C. *et al.* Water-Processable Polymer–Nanocrystal Hybrids for Thermoelectrics. *Nano Lett.* **10**, 4664–4667 (2010).
2. Russ, B., Glaudell, A., Urban, J. J., Chabinyc, M. L. & Segalman, R. A. Organic thermoelectric materials for energy harvesting and temperature control. *Nature Reviews Materials* vol. 1 1–14 (2016).
3. Zaia, E. W., Gordon, M. P., Yuan, P. & Urban, J. J. Progress and Perspective: Soft Thermoelectric Materials for Wearable and Internet-of-Things Applications. *Adv. Electron. Mater.* **5**, 1800823 (2019).
4. Fan, Z. & Ouyang, J. Thermoelectric Properties of PEDOT:PSS. *Advanced Electronic Materials* vol. 5 1–23 (2019).
5. Kumar, P. *et al.* Polymer morphology and interfacial charge transfer dominate over

energy-dependent scattering in organic-inorganic thermoelectrics. *Nat. Commun.* **9**, 5347 (2018).

6. Chen, Y., Zhao, Y. & Liang, Z. Solution processed organic thermoelectrics: towards flexible thermoelectric modules. *Energy Environ. Sci.* **8**, 401–422 (2015).

7. Bahk, J.-H., Fang, H., Yazawa, K. & Shakouri, A. Flexible thermoelectric materials and device optimization for wearable energy harvesting. *J. Mater. Chem. C* **3**, 10362–10374 (2015).

8. Siddique, A. R. M., Mahmud, S. & Heyst, B. Van. A review of the state of the science on wearable thermoelectric power generators (TEGs) and their existing challenges. *Renewable and Sustainable Energy Reviews* vol. 73 730–744 (2017).

9. Park, S.-I. *et al.* Light Emission Characteristics and Mechanics of Foldable Inorganic Light-Emitting Diodes. *Adv. Mater.* **22**, 3062–3066 (2010).

10. Kim, S. *et al.* Low-power flexible organic light-emitting diode display device. *Adv. Mater.* **23**, 3511–3516 (2011).

11. Coates, N. E. *et al.* Effect of interfacial properties on polymer-nanocrystal thermoelectric transport. *Adv. Mater.* **25**, 1629–1633 (2013).

12. See, K. C. *et al.* Water-processable polymer-nanocrystal hybrids for thermoelectrics. *Nano Lett.* **10**, 4664–4667 (2010).

13. Coates, N. E. *et al.* Effect of Interfacial Properties on Polymer-Nanocrystal Thermoelectric Transport. *Adv. Mater.* **25**, 1629–1633 (2013).

14. Yee, S. K., Coates, N. E., Majumdar, A., Urban, J. J. & Segalman, R. A. Thermoelectric power factor optimization in PEDOT:PSS tellurium nanowire hybrid composites. *Phys.*

Chem. Chem. Phys. **15**, 4024–4032 (2013).

15. Jin Bae, E., Hun Kang, Y., Jang, K. S. & Yun Cho, S. Enhancement of Thermoelectric Properties of PEDOT:PSS and Tellurium-PEDOT:PSS Hybrid Composites by Simple Chemical Treatment. *Sci. Rep.* **6**, 1–10 (2016).
16. Yang, L. *et al.* Decoupling electron and phonon transport in single-nanowire hybrid materials for high-performance thermoelectrics. *Sci. Adv.* **7**, eabe6000 (2021).
17. Zaia, E. W. *et al.* Carrier Scattering at Alloy Nanointerfaces Enhances Power Factor in PEDOT:PSS Hybrid Thermoelectrics. *Nano Lett.* **16**, 3352–3359 (2016).
18. Song, H. & Cai, K. Preparation and properties of PEDOT:PSS/Te nanorod composite films for flexible thermoelectric power generator. *Energy* **125**, 519–525 (2017).
19. Culebras, M. *et al.* Manufacturing Te/PEDOT Films for Thermoelectric Applications. *ACS Appl. Mater. Interfaces* **9**, 20826–20832 (2017).
20. Heyman, J. N. *et al.* Terahertz and infrared transmission of an organic/inorganic hybrid thermoelectric material. *Appl. Phys. Lett.* **104**, 141912 (2014).
21. Gregory, S. A. *et al.* Effect of Heteroatom and Doping on the Thermoelectric Properties of Poly(3-alkylchalcogenophenes). *Adv. Energy Mater.* **8**, 1802419 (2018).
22. Gregory, S. A. *et al.* Quantifying charge carrier localization in chemically doped semiconducting polymers. *Nat. Mater.* 1–8 (2021) doi:10.1038/s41563-021-01008-0.
23. Gordon, M. P. *et al.* Microstructure and heteroatom dictate the doping mechanism and thermoelectric properties of poly(alkyl-chalcogenophenes). *Appl. Phys. Lett.* **118**, 233301 (2021).
24. Walzer, K., Männig, B., Pfeiffer, M. & Leo, K. Highly efficient organic devices based on

electrically doped transport layers. *Chemical Reviews* vol. 107 1233–1271 (2007).

25. Cochran, J. E. *et al.* Molecular interactions and ordering in electrically doped polymers: Blends of PBTTT and F4TCNQ. *Macromolecules* **47**, 6836–6846 (2014).

26. Winokur, M. *et al.* X-ray scattering from sodium-doped polyacetylene: Incommensurate-commensurate and order-disorder transformations. *Phys. Rev. Lett.* **58**, 2329–2332 (1987).

27. Schlitz, R. A. *et al.* Solubility-limited extrinsic n-type doping of a high electron mobility polymer for thermoelectric applications. *Adv. Mater.* **26**, 2825–2830 (2014).

28. Shi, K. *et al.* Toward High Performance n-Type Thermoelectric Materials by Rational Modification of BDPPV Backbones. *J. Am. Chem. Soc.* **137**, 6979–6982 (2015).

29. Huang, J. *et al.* Investigation of the effects of doping and post-deposition treatments on the conductivity, morphology, and work function of poly(3,4-ethylenedioxythiophene)/poly(styrene sulfonate) films. *Adv. Funct. Mater.* **15**, 290–296 (2005).

30. Vitoratos, E. Conductivity Degradation Study of PEDOT: PSS Films under Heat Treatment in Helium and Atmospheric Air. *Open J. Org. Polym. Mater.* **02**, 7–11 (2012).

31. Aasmundtveit, K. E. *et al.* Structure of thin films of poly(3,4-ethylenedioxythiophene). *Synth. Met.* **101**, 561–564 (1999).

32. Zhou, J. *et al.* The temperature-dependent microstructure of PEDOT/PSS films: Insights from morphological, mechanical and electrical analyses. *J. Mater. Chem. C* **2**, 9903–9910 (2014).

33. W Wolfe, R. M. *et al.* Simultaneous Enhancement in Electrical Conductivity and Thermopower of n-Type NiETT/PVDF Composite Films by Annealing. *Adv. Funct.*

Mater. **28**, 1803275 (2018).

34. Menon, A. K. *et al.* Progress in Nickel-Coordinated Polymers as Intrinsically Conducting n-Type Thermoelectric Materials. *Adv. Electron. Mater.* **5**, 1800884 (2019).

35. Loo, J. S. C., Ooi, C. P. & Boey, F. Y. C. Degradation of poly(lactide-co-glycolide) (PLGA) and poly(L-lactide) (PLLA) by electron beam radiation. *Biomaterials* **26**, 1359–1367 (2005).

36. Ma, J. *et al.* Thermal conductivity of electrospun polyethylene nanofibers. *Nanoscale* **7**, 16899–16908 (2015).

37. Chaudhary, N. *et al.* Electron beam induced modifications in electrical properties of Poly(3,4-ethylenedioxythiophene):poly(styrenesulfonate) films. *Vacuum* **152**, 243–247 (2018).

38. Shi, L. *et al.* Measuring thermal and thermoelectric properties of one-dimensional nanostructures using a microfabricated device. *J. Heat Transfer* **125**, 881–888 (2003).

39. Yang, L. *et al.* Thermal conductivity of individual silicon nanoribbons. *Nanoscale* **8**, 17895–17901 (2016).

40. Yang, L. *et al.* Ballistic Phonon Penetration Depth in Amorphous Silicon Dioxide. *Nano Lett.* **17**, 7218–7225 (2017).

41. Yang, L. *et al.* Distinct Signatures of Electron–Phonon Coupling Observed in the Lattice Thermal Conductivity of NbSe3 Nanowires. *Nano Lett.* **19**, 415–421 (2019).

42. Yang, L. Phonon Transport in Nanowires–Beyond Classical Size Effects. *Ph.D. thesis, Vanderbilt Univ.* (2019).

43. Yang, L., Zhao, Y., Zhang, Q., Yang, J. & Li, D. Thermal transport through fishbone

silicon nanoribbons: Unraveling the role of Sharvin resistance. *Nanoscale* **11**, 8196–8203 (2019).

44. Yang, L. *et al.* Kink as a new degree of freedom to tune the thermal conductivity of Si nanoribbons. *J. Appl. Phys.* **126**, 155103 (2019).

45. Epstein, A. S., Fritzsche, H. & Lark-Horovitz, K. Electrical properties of tellurium at the melting point and in the liquid state. *Phys. Rev.* **107**, 412–419 (1957).

46. Patel, S. N. *et al.* Morphology controls the thermoelectric power factor of a doped semiconducting polymer. *Sci. Adv.* **3**, e1700434 (2017).

47. Shen, S., Henry, A., Tong, J., Zheng, R. & Chen, G. Polyethylene nanofibres with very high thermal conductivities. *Nat. Nanotechnol.* **5**, 251–255 (2010).

48. Dongmin Kang, S. & Jeffrey Snyder, G. Charge-transport model for conducting polymers. *Nat. Mater.* **16**, 252–257 (2017).

49. Wang, X. *et al.* High electrical conductivity and carrier mobility in oCVD PEDOT thin films by engineered crystallization and acid treatment. *Sci. Adv.* **4**, eaat5780 (2018).

50. WRIGHT, D. A. Thermoelectric Properties of Bismuth Telluride and its Alloys. *Nature* **181**, (1958).

51. Bubnova, O. *et al.* Optimization of the thermoelectric figure of merit in the conducting polymer poly(3,4-ethylenedioxythiophene). *Nat. Mater.* **10**, 429–433 (2011).

52. Bubnova, O. *et al.* Semi-metallic polymers. *Nat. Mater.* **13**, 190–194 (2014).

53. Gordon, M. P. *et al.* Understanding Diameter and Length Effects in a Solution-Polystyrene Sulfonate Hybrid Thermoelectric Nanowire Mesh. *Adv. Electron. Mater.* **2000904**, 1–6 (2021).